Immunity Study: Port Impedance Measurement of PMU and PCI Testing Under EMP

Liang Zhang, *Member, IEEE*, Wei Qiu, *Member, IEEE*, He Yin, *Senior Member, IEEE*, Kaiqi Sun, *Member, IEEE*, Lawrence C Markel, *Member, IEEE*, DaHan Liao, *Member, IEEE*, Zhi Li, *Member, IEEE*, Ben W Mcconnell, *Senior Member, IEEE*, and Yilu Liu, *Fellow, IEEE*

***Abstract*—With the increased requirements of real-time grid monitoring, disturbance location, and situation awareness, Phasor Measurement Units (PMUs) have become more critical for the Wide Area Measurement System (WAMS). However, the vulnerability of PMUs has not been well studied, especially under electromagnetic pulse (EMP) scenarios. The stable operation of the power system will be affected directly once EMP damages them. Therefore, studying their immunity to EMP events is urgent and necessary. In this article, the effective impedance measurement scheme and pulsed current injection (PCI) testing are proposed for the port impedance measurement and immunity levels of PMUs. The equivalent non-uniform transmission line model is established to eliminate the impact of the fixture in the de-embedding process. Then, the circuit of the pulsed current generator is set to generate a damping sinusoid, and the double exponential wave is applied to the port. Finally, using measured impedance as a generator load, the voltage and current responses of different ports are calculated in the PCI testing simulation. Results reveal the characteristics of port impedance, waveforms of voltage and current, and distribution of accumulative energy. The relation between port impedance and the waveforms is discussed.**

***Index Terms*—Phasor measurement units (PMU), electromagnetic pulse (EMP), impedance measurement, pulsed current injection (PCI).**

I. Introduction

THE development of high penetration of distributed renewable energy sources has increased the monitoring demand for distributed power grids. Phasor Measurement Units (PMU) that can measure the real-time synchrophasor data and stream back to the Wide Area Monitoring System (WAMS), are critical for the grid monitoring, disturbance location, and situation awareness of WAMS [1], [2]. Currently, more than 2000 PMUs have been deployed in the United States, which are distributed in different nodes of the power grid [3]. Therefore, the reliability of the PMU directly affects the stable operation and control of the power system. The experiences of extreme weather have improved the resilience of the WAMS system [4]. However, few studies have focused on the stability and reliability of PMU under the Electromagnetic Pulse (EMP), where the EMP is a type of short burst of electromagnetic energy. The EMP can be easily coupled to PMU through transmission lines and antennas (GPS receivers), thereby damaging the circuit of the equipment. Once the induced current and voltage are measured, effective measures can be taken to defend against the EMP.

The EMP typically contains three stages, including the early time E1 peaking at about 50 kV/m and decaying to nearly zero within 0.1us, E2 with a strong close to lightning, and E3 with a strength similar to the solar wind or geomagnetic storm. There is various research about the effect of E2 and E3 [5]. However, the E1 of EMP has the highest energy intensity, and the research on power grids for E1 is extremely limited. For example, the Soviet Union and the United States tested the high attitude of air-explosive in 1961 and 1962, respectively. The test found that the power electronic equipment of the electronic systems was damaged even 3,000 kilometers away [6]. Therefore, it is urgent and necessary to provide an effective way to evaluate grid consequences from EMP. The primary objective of this article is to study the immune response of PMU under EMP [7].

To study the immune response of electronic devices under EMP, different testing methods are proposed accordingly. Basically, totally three tested methods are developed, including the Electromagnetic Environments Simulator (EES), hardware-based pulsed current injection (PCI) test, and the simulation.

Generally, immunity levels of equipment to EMP can be measured by a radiative test, which can be achieved by EES. EES needs a large power impulse source and should put the device under an EMP environment, so it is not easy to carry out. In [8], a multigap loop antenna and the low-noise norm detector are designed to measure the ns-level magnetic-field. Similarly, in [9], a free field illumination test setup is built to test the bulk power system based on MIL-STD- 461 G/RS105 [10], where the

Manuscript received 24 December 2022; revised 30 May 2023; accepted 10 July 2023. Date of publication 17 July 2023; date of current version 22 November 2023. Paper 2022-PSEC-1644.R1, presented at the 2022 IEEE/IAS Industrial and Commercial Power System Asia, Shanghai, China, Jul. 08–11, and approved for publication in the IEEE Transactions on Industry Applications by the Power Systems Engineering Committee of the IEEE Industry Applications Society [DOI: 10.1109/ICPSAsia55496.2022.9949880]. This work was supported in part by the DOE Grid Modernization Lab Call (GMLC) Project: Vulnerability of Power Generation Critical Systems Against Electromagnetic Threats under Grant 36129, and in part by CURENT Industry Partnership Program. *(Corresponding author: Wei Qiu.)*

Liang Zhang, Wei Qiu, He Yin, and Kaiqi Sun are with the Department of Electrical Engineering, and Computer Science, The University of Tennessee, Knoxville, TN 37996 USA (e-mail: liangzhangswpu@gmail.com; qwei4@utk.edu; hyin8@utk.edu; ksun8@utk.edu).

Lawrence C Markel, DaHan Liao, Zhi Li, and Ben W Mcconnell are with the Oak Ridge National Laboratory, Oak Ridge, TN 37831 USA (e-mail: markellc@ornl.gov; liaod@ornl.gov; liz2@ornl.gov; liz2@ornl.gov).

Yilu Liu is with the Department of Electrical Engineering and Computer Science, The University of Tennessee, Knoxville, TN 37996 USA, and also with the Oak Ridge National Laboratory, Oak Ridge, TN 37831 USA (e-mail: liu@utk.edu).

Color versions of one or more figures in this article are available at https://doi.org/10.1109/TIA.2023.3296394.

Digital Object Identifier 10.1109/TIA.2023.3296394

fiber optic cables control the EMP-hardened camera. Besides, an EES named Gigahertz Transverse Electromagnetic Simulator (GTEM) was built at Sandia National Laboratories [11]. The GTEM can be used to measure the equipment susceptibility and it can test the devices with a spectrum of DC to GHz frequencies. The advantage of the EES is that it can construct the environment closest to the actual electromagnetic field. The tested results of EES are reliable. However, constructing this simulator would consume extremely high precision and expensive equipment.

To this end, immunity testing is designed for intense electromagnetic pulses based on the hardware-based PCI test. PCI test is a good replacement for EES and is usually used in conducted immunity tests. For example, a PCI test setup is established in [12] and [13]. The critical parameters of the pulse generator can be adjusted in this test setup. This PCI test consists of exponential pulse generators, injecting probe, the attenuator, the equipment under test, a monitor probe, as well as an oscilloscope. The study in [14] developed two procedures, including a black-box approach and interpretation of coupling and propagation effects, to address the issue of circuit characterization of bulk injection probes. The radiated susceptibility of the antenna systems is assessed based on the pulsed differential-mode current injection method [15]. It is a simple and straightforward method to study the vulnerability of electronic devices. Nonetheless, the frequency range and nonlinear transfer function between the cable currents and radiated field might limit the effectiveness of the PCI testing [16].

Apart from the above hardware-based testing, the simulation provides a software-based solution. It can avoid measurement errors and is suitable for large-scale system applications, such as large wind and photovoltaic (PV) farms. In [17], the transient overvoltage is derived from controlling the internal surges of large PV farms based on the EMTP-RV/MATLAB. The finite-difference time-domain (FDTD) method is a powerful tool for modeling nano-scale electromagnetic field analysis. The lightning stroke is reproduced in [18] to study the effect of the overvoltage on the DC side. Meanwhile, the frequency-domain method can be used to simulate the voltage and current responses based on the measured impedance [19]. However, the frequency range of the measuring equipment and the de-embedding process in the simulation will be obstacles to the accurate immunity study for power electronic equipment such as PMU.

Currently, the immunity studies of some typical grid infrastructures, such as the PV panel, inverters [20], transformer [21], and coaxial cable, have been tested. The monitoring devices PMU have not been well studied, which serve as the key link in power systems.

To address the above-mentioned problem, this manuscript proposes an effective impedance measurement and pulsed current injection testing scheme for the port impedance measurement and immunity levels of PMUs considering the numerous ports and varying degrees of immunity guidelines. And its an extension of the conference article in 2022 I&CPS Asia [22]. The proposed scheme has the characteristics of wide bandwidth, low cost, and flexibility. The contributions of this article can be summarized below:

1) First, the impedance of different ports of PMU is measured by two network analyzers and an LCR meter, where the advantage is that a wider frequency can be measured from 40 Hz to 1.3 GHz. A de-embedding solution is further developed to eliminate the effect of the fixture. The impedance will then be used in the immunity study.
2) Then, the pulse current generators are established to output pulsed current and voltage. The advantage is that it is flexible and low-cost to test the immunity responses according to IEC standard levels. The induced current and voltage can be well estimated.
3) Finally, transient responses under EMP for typical ports are calculated and analyzed by using port impedance as the load of the generator. The spectrum and cumulative energy are also analyzed to study the vulnerability of different ports.

The content of this article is as follows. Section II introduces the impedance measurement for PMU. De-embedding and data integration of impedance measurement results is presented in Section III. Thereafter, the PCI method is introduced in Section IV. Different experiments are conducted in Section V. The conclusion is drawn in Section VI.

Fig. 1. Impedance measurement instruments.

TABLE I
FEATURES OF THREE IMPEDANCE MEASURING INSTRUMENTS

	LCR meter	Imp. Analyzer	VNA
Name	MCR-5200	HP 4395A	Planar TR1300/1
Manufacturer	Matrix Technology	Agilent Technologies	Copper Mountain Technologies
Adapter	-	HP 87512A	N1.1 Calibration Kit
Freq. range	40Hz-200kHz	10Hz-500MHz	300kHz-1.3GHz
Imp. range	$0.1\text{m}\Omega - 99.99\text{M}\Omega$	$< 40\text{k}\Omega$	-
Accuracy	$> 0.1\%$	3%-10%	0.5%-3%

II. IMPEDANCE MEASUREMENT

To achieve the PCI response of PMU, the first step is to obtain effective impedance values. Considering that electromagnetic pulses can occur in electric or magnetic field of different strengths in different directions, they typically comprise a wide frequency range from a low (Hz level) to a high value (GHz level). The impedance measurement devices should have a wide measurement interval. However, most measuring instruments can only provide a specific range of values. Therefore, three instruments are used together to obtain the actual impedance results depending on their frequency ranges in this Section.

The evaluation of these three instruments is listed in Fig. 1 and Table I. The LCR meter is one type of commonly used device to measure inductance (L), capacitance (C), and resistance (R) [23]. A network analyzer (NA) is an instrument that measures the network parameters of electrical networks [24]. It commonly

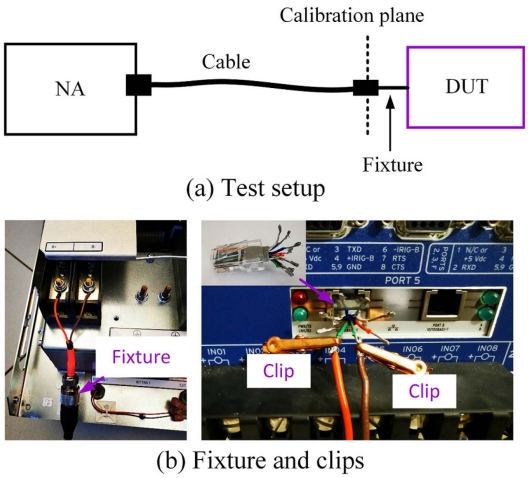

Fig. 2. Impedance measurement using a network analyzer.

measures s-parameters because reflection and transmission are easy to measure at high frequencies.

Based on the measured reflection coefficient S_{11}, the impedance can then be calculated using the equation [24].

$$Z_{eff} = \sqrt{\frac{(1+S_{11})^2 - S_{21}^2}{(1-S_{11})^2 - S_{21}^2}} \tag{1}$$

where S_{21} is the forward voltage gain, it can be safely set to zero if only one port is used in the vector network analyzer (VNA). Both the LCR meter and impedance analyzer can directly measure the impedance and output the values at different frequencies.

As listed in Table I, the network analyzers we use are from Copper Mountain Technologies (Planar TR1300/1) and Agilent (HP 4395 A), which are both famous manufacturers in the world. The network analyzer works based on the frequency sweep analysis mode. Planar TR1300/1 sweeps from 300 kHz to 1.3 GHz. The sweep type is chosen to be linear and sweep points are set to a maximum of 16001. HP 4395 A sweeps from 10 Hz to 500 MHz with 805 points. However, it has a limitation of 40 kΩ measurement range. LCR meter (MCR-5200) provides a supplementary measurement for the large impedance of the low-frequency part. It manually measures 41 points from 40 Hz to 200 kHz. This means that the Planar TR1300/1 and HP 4395 A have a higher resolution compared with the LCR meter. And the data from the three instruments are fused together to achieve a wide bandwidth measurement.

To ensure consistent results, the output voltages of the three instruments are all set to a relatively low value, 0.1 V. The corresponding output power is −7 dBm. The impedance measurement using a network analyzer is demonstrated in Fig. 2.

In Fig. 2(a), calibration is done at the end of the cable, and a fixture is needed to connect the device under test (DUT, namely PMU) and the cable. Fig. 2(b) shows the actual connections between the fixture and ports. For some ports such as network and serial connections, clips are helpful in the connection between fixtures and wires.

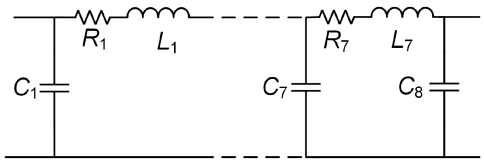

Fig. 3. Non-uniform transmission line model for de-embedding based on the fixture.

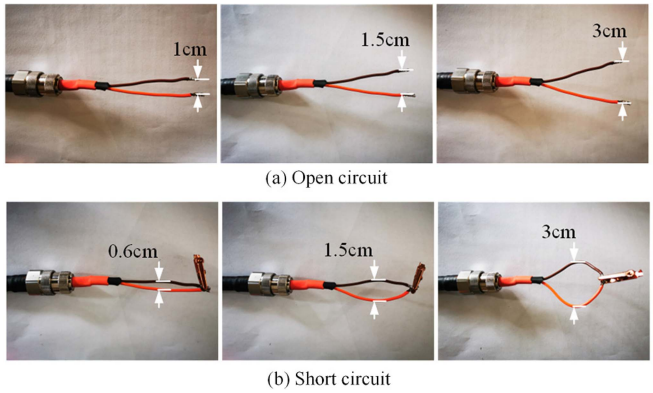

Fig. 4. Open and short impedance measurement of different df.

The measurement results contain the impedance from both the PMU port and the fixture. This may bring some errors when measuring relatively large or small impedance values, especially in the high frequency part. Therefore, the de-embedding process is necessary to eliminate the influence of the fixture [25].

III. De-Embedding for the Raw Measuring Values

To obtain the actual impedance of PMU ports, the commonly used de-embedding method is the open-short and short-open de-embedding method [26]. It has an effective effect in the low-frequency part. However, it should be noted that the wires between the ground and the signal also have resistance and inductance in the short pattern, leading to bias at high frequencies. In this section, a de-embedding method is established to eliminate the impact of fixtures based on the non-uniform transmission line model.

To this end, a seven-stage cascade of the transmission line model is designed, as depicted in Fig. 3, which is the equivalent circuit of the fixture. The left side is connected to the cable and the right side is connected to DUT. Resistance, inductance, and capacitance are the three main parameters of the fixture. To obtain these parameters, the total parallel capacitance and serial inductance are estimated based on measured open and short circuit impedance.

Basically, wire distance d_f will affect both the capacitance and inductance of the fixture. The impedance of several conditions shown in Fig. 4 is measured.

The total capacitance can be calculated using $C_t = -1/(2\pi f X_c)$, where f and X_c are the frequency (Hz) and the capacitive reactance (Ω), respectively. Similarly, the total serial

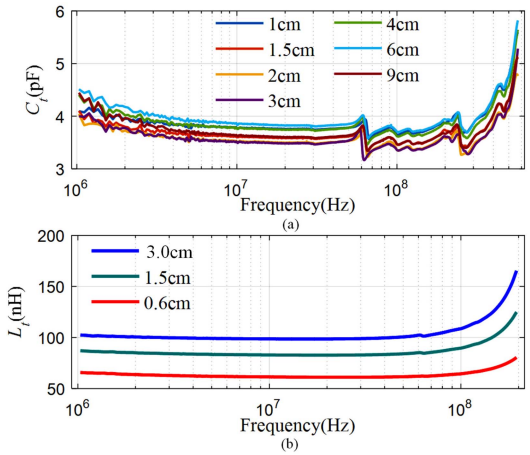

Fig. 5. Calculated total capacitance and inductance C_t and L_t in different d_f. (a) Capacitance, (b) Inductance.

TABLE II
DISTRIBUTION OF CAPACITORS AND INDUCTORS IN THE SEVEN-STAGE CASCADE OF TRANSMISSION LINE MODEL

Stage	1	2	3	4	5	6	7	8
C_i(pF)	1.8	0.7	0.5	0.25	0.15	0.1	0.09	0.07
l_i(nH)	7.4	9.5	12.3	12.3	12.3	12.3	12.3	-

inductance can be calculated as $L_t = X_l/(2\pi f)$ based on the short circuit, where X_l is the inductive reactance.

The C_t and L_t with distances $d_f \in 0.6\,\text{cm} - 3\,\text{cm}$ are tested and calculated, as demonstrated in Fig. 5. The capacitance is changing with the distance between two wires. The mean value can be obtained and is located from 3.48 pF to 3.83 pF for the flat part. Considering that the distance between wires is usually about 2 cm, the average capacitance C_t is set to 3.7 pF. Meanwhile, the total serial inductance L_t is distributed in 60nH to 100nH when f is lower than 100 MHz. The average value is set to 80nH. The resistance of the non-uniform transmission line model can be obtained from the short circuit impedance.

The next step is for estimating the detailed capacitance and inductance values for each stage transmission line model. Generally, the capacitance and inductance of the transmission line model can be expressed as (2).

$$C_i = \frac{\pi\varepsilon}{\ln\frac{d_f}{2r}}$$
$$L_i = \frac{\mu_0}{4\pi} + \frac{\mu_0}{\pi}\left(\ln\frac{d_f - r}{r}\right) \tag{2}$$

where μ_0 denotes the vacuum permeability, r is the wire radius of the fixture, ε is the relative permittivity, $i = 1, 2, \ldots, 7$.

The motivation of estimate the C_i and L_i are to minimize the impedance errors between the measurement and the equivalent circuit. Based on the resonance points, trial and errors, the estimated C_i and L_i are estimated and listed in Table II.

Fig. 6 indicates the measured and calculated open circuit impedance of the fixture. They are consistent both in amplitude and phase. This is a verification of the transmission line model of the fixture.

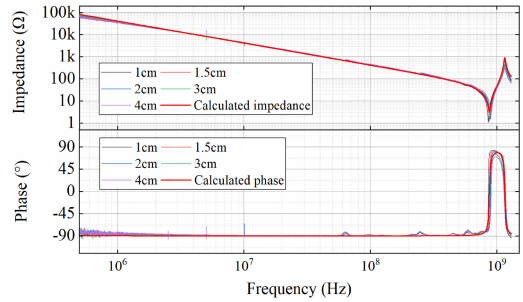

Fig. 6. Open and short impedance measurement of different d_f.

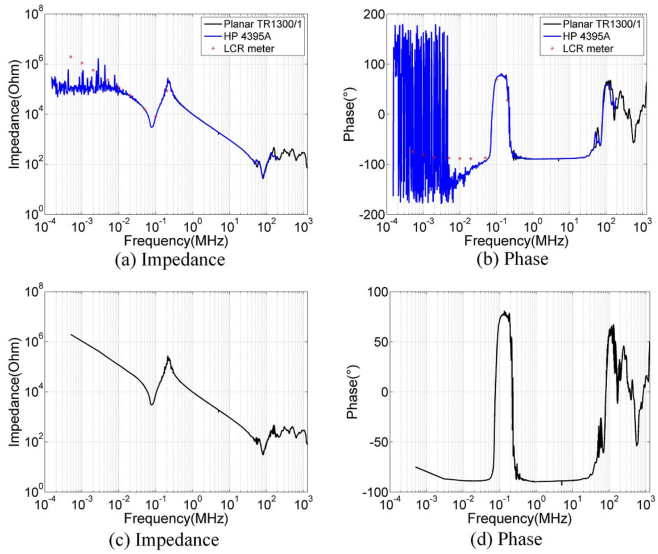

Fig. 7. Impedance measurement results and integrated results.

After de-embedding is completed, the measured impedance needs to be further integrated since there are three sets of measurement results. This is achieved by curve fitting and interpolation. An example of port impedance measurement results and combination is shown in Fig. 7.

Fig. 7(a) is the absolute value and phase of port impedance measured by three instruments. In the low-frequency part, values have exceeded the measurement range of NA. To address this issue, the LCR meter is used and it can provide the correct values. Fig. 7(b) illustrates the integrated results of impedance.

IV. PULSED CURRENT INJECTION RESPONSE ANALYSIS OF PMU

To explore the response of the PMUs under high-altitude electromagnetic pulse (HEMP), the coupling mechanism has been proposed using the circuit network. For example, the probe is modeled as the transformer in [27]. And the current distributions are with reasonable accuracy. The advantages of PCI are its simplicity and ease of control [16]. Therefore, the E1 of HEMP coupling is emulated via the PCI method.

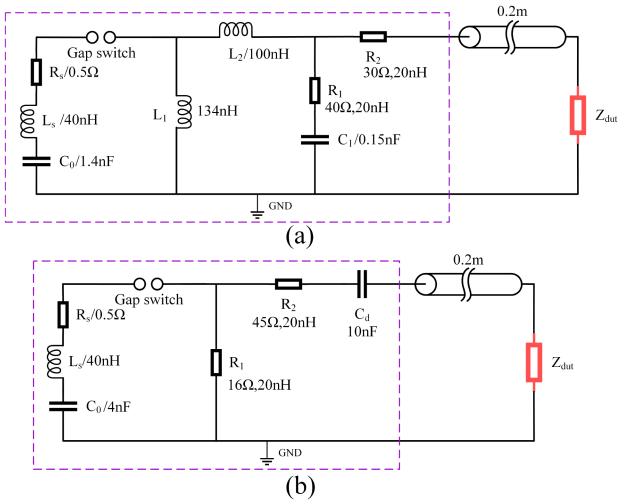

Fig. 8. The circuit diagram of the PCI test. (a) EC5 level, (b) EC8 level.

TABLE III
PARAMETER REQUIREMENTS FOR DAMPED SINUSOIDS UNDER EC5

Output type	Rise time	Oscillation Frequency	Decaying
Open circuit	$5ns \pm 30\%$	$(3, 10, 30)MHz \pm 10\%$	$P_{k5} > 50\%P_{k1}$
voltage	-	-	$P_{k10} < 50\%P_{k1}$
Short circuit	$3MHz :< 330ns$	$(3, 10, 30)MHz \pm 30\%$	$P_{k5} > 25\%P_{k1}$
current	$10MHz :< 100ns$	-	$P_{k10} < 25\%P_{k1}$
	$30MHz :< 33ns$	-	-

TABLE IV
PARAMETER REQUIREMENTS FOR DOUBLE EXPONENTIAL WAVEFORMS UNDER EC8

Load resistance	Rise time	Pulse width	Peak voltage
50Ω	$(5 \pm 1.5)ns$	$(50 \pm 15)ns$	$4kV \pm 10\%$
1000Ω	$(5 \pm 1.5)ns$	$50ns(-15ns$ to $+100ns)$	$7.6kV \pm 20\%$

The simplified circuit diagram of PCI is presented in Fig. 8 based on IEC 61000-4-25 [28].

Although there are twelve immunity test levels, basically, two types of output waveforms are adopted, namely damped sinusoids for lower EC1-EC6 levels and double exponential waveforms for higher six levels [28], [29].

Here EC5 level and EC8 level are selected and simulated, the requirements of waveform parameters for damped sinusoids and double exponential waveforms are shown in Table III according to IEC 61000-4-4 [30] and Table IV according to IEC 61000-4-18 [31].

For damped sinusoids, parameters are rise time, oscillation frequency, decaying, and peak value. The peak value under EC5 is $2kV \pm 10\%$ for open circuit voltage and $40A \pm 20\%$ for short circuit current. For double exponential waveforms, parameters are rise time, pulse width, and peak voltage. Peak voltage under EC8 should be about 4 kV in 50Ω load and 7.6 kV in 1000Ω load.

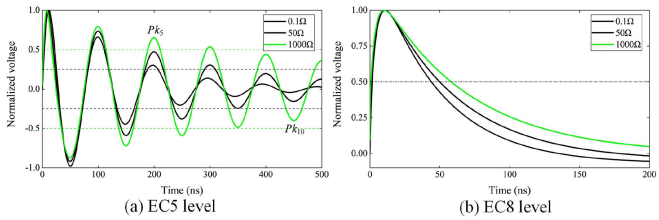

Fig. 9. Normalized output waveforms of the generator.

The simplified circuit diagram of PCI is presented in Fig. 8 based on IEC 61000-4-25 [28]. The circuit in the dashed box represents the pulse current generator. Parameters shown in the figure ensure that the output waveforms meet the requirements of IEC standard. The output of the generator is connected to impedance Z_{dut} through a 50 Ω coaxial cable. Z_{dut} represents the measured port impedance of PMU. When the gap switch is triggered, a pulse voltage is applied to the circuit. The voltage and current waveforms on the load are calculated in the frequency domain, and then converted to the time domain. All calculations are done by Matlab code.

For the EC5 level, there are three oscillation frequencies: 3 MHz, 10 MHz, and 30 MHz. 10 MHz waveform is illustrated and the normalized waveforms are demonstrated in Fig. 9(a) for typical load of 0.1 Ω, 50 Ω, and 1000 Ω. With the main capacitor charged to 2.3 kV, the short current is 40 A and the open voltage is 2000 V. Similarly, normalized waveforms of the EC8 level are shown in Fig. 9(b). With the main capacitor charged to 9.05 kV, the short current is 160 A and the open voltage is 8 kV.

V. EXPERIMENT RESULTS

This section shows the impedance measurement results of PMU and PCI simulation results.

A. Impedance Measurement Results of PMU

In this section, three PMUs are tested, including the transmission level-based PMU Model 1133 A, and distribution level PMUs micro-PMU PQube 3 and Universal Grid Analyzer (UGA). It should be noted that the network analyzer and LCR meter are commonly used devices in the immunity study under electromagnetic pulse. In terms of product design and protection, the vulnerability of the industrially deployed PMUs can be evaluated by the PCI model with the measured impedance. The measured PMUs and ports are demonstrated in Figs. 10 and 13. All instruments are warmed up for one hour before measurement.

Here power input, analog input (E), and RJ-45 ethernet port (I) shown in Fig. 11(b) are selected to be analyzed. It should be noted that the ethernet port is 48 V PoE (Power over Ethernet) compatible. Connecting an ethernet cable to a PoE port can power the μPMU.

As there are common mode and differential mode disturbances, wire-ground and wire-wire impedance are both measured. The impedance of the wire-ground results is presented in Fig. 12. For the ethernet port, there are four pairs of wires inside

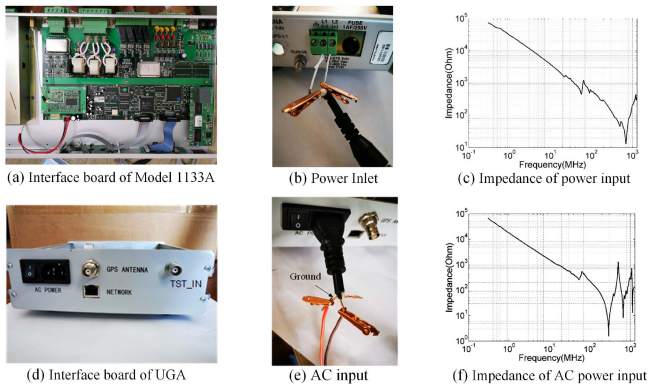

Fig. 10. (a) and (b) Transmission level Model 1133 A, (c) impedance of power input for Model 1133 A, (d) and (e) Distribution level PMU UGA, (f) impedance of power input for UGA.

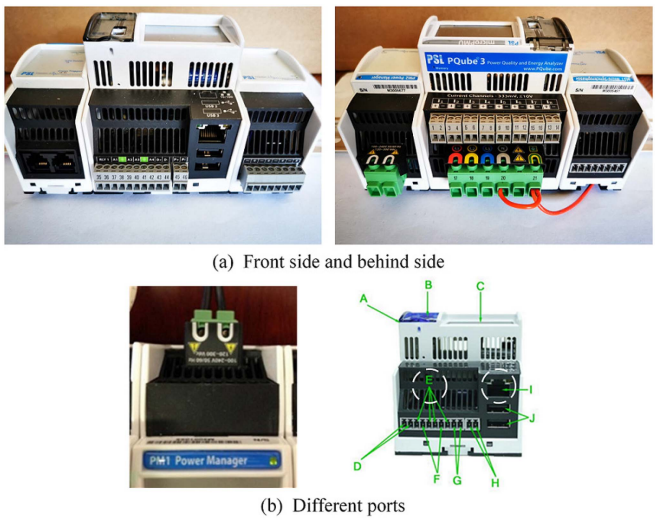

Fig. 11. The measured μPMU and ports.

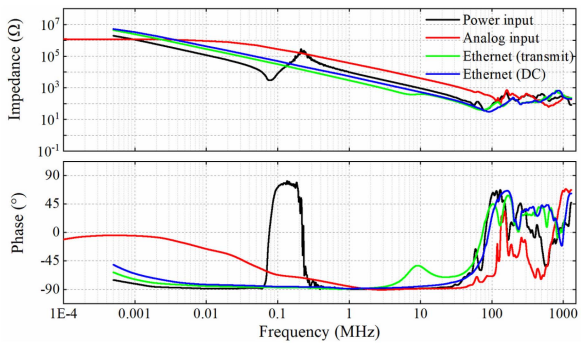

Fig. 12. The measured wire-ground impedance of different ports.

the cable, and two of the results are listed here for transmit and DC wire pairs. Compared with the measured impedance as presented in Fig. 13, they have a similar impedance profile.

It can be seen from Fig. 12 that there are some differences in the curve for different ports but wire-ground impedance always shows up as large values. It exceeds 1 MΩ in the low-frequency

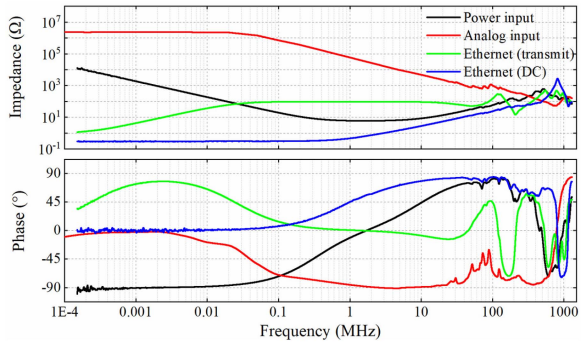

Fig. 13. The measured wire-wire impedance of different ports.

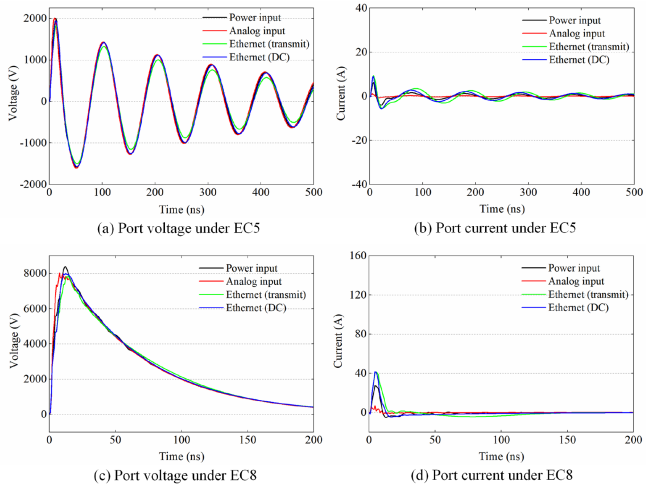

Fig. 14. Common mode voltage and current response for different ports.

part and at least several 100's Ω up to 10 MHz. And the impedance is mainly capacitive up to 100 MHz as phase is negative, except for power port near 0.1 MHz. For analog input port, phase goes to zero at 1 kHz and there should be parallel resistor for the port whose resistance is about 1 MΩ.

Similarly, the wire-wire impedance results of different ports are further presented in Fig. 13. For analog input ports, wire-wire impedance is still a large value, which means ports are isolated from each other. However, the impedance of the other three ports is much lower, actually no more than 100 Ω in a large frequency range, and phase changes with frequency. For the power input port, the impedance will drop fast from 10 $k\Omega$ to several Ω at about 1 MHz and then increase to several 100's Ω. For ethernet (transmit) port, impedance increase to 100 Ω and keep stable in a large frequency range. For ethernet port (DC), impedance is lower than 20 Ω below 100 MHz.

B. Results of Pulsed Current Injection Response

Based on the circuit of PCI and measured port impedance, voltage and current response for the selected ports can be calculated for EC5 and EC8 immunity levels. The voltage and current waveforms of the common mode are illustrated in Fig. 14.

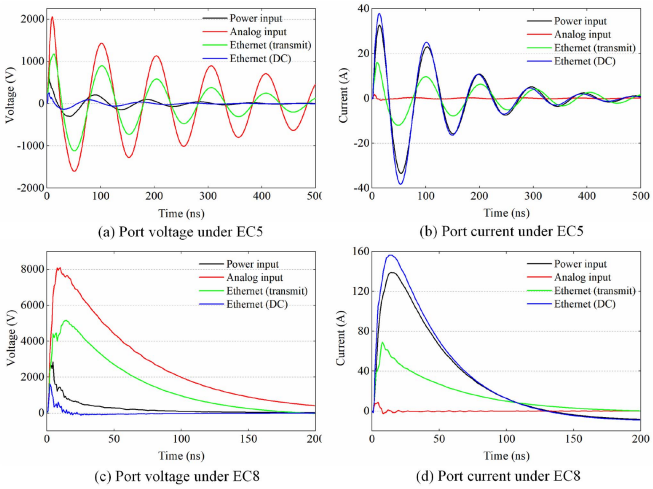

Fig. 15. Differential mode voltage and current response for different ports.

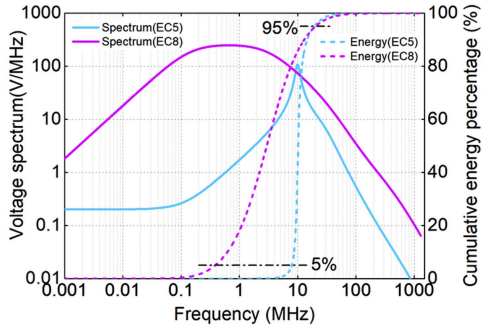

Fig. 16. Voltage spectrum and cumulative energy of EC5 and EC8.

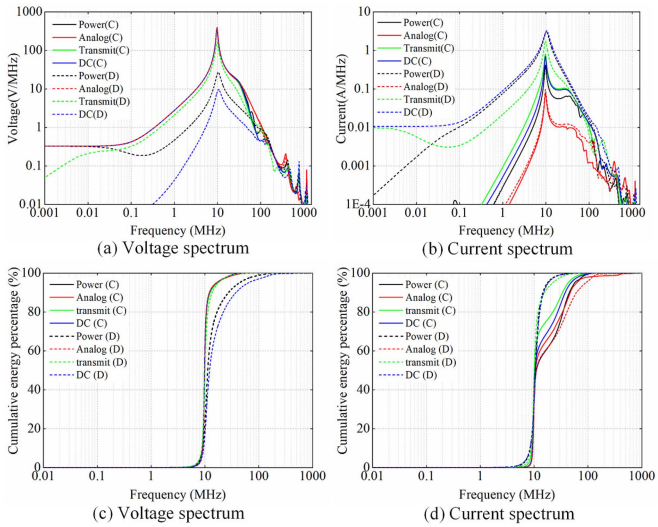

Fig. 17. Spectrum and cumulative energy of voltage and current under EC5.

It can be found from Fig. 14 that the peak values of voltage for different ports are very close to the open voltage of the generator. It is 2 kV and 8 kV for EC5 and EC8 levels, respectively. Current is several amperes to 10's amperes and wave width is only about 10 ns.

Voltage and current waveforms of differential mode are demonstrated in Fig. 15. For the analog port, the results should be similar to Fig. 14 since the impedance is similar. For the power and ethernet (DC) port, the voltage is small, and the current is close to the short current of the generator, 40 A under EC5 and 160 A under EC8. This is mainly caused by the small port impedance. And the pulse width of the voltage is much narrower than that of current waveform. For ethernet (transmit) port, due to the stable impedance of 100 Ω in a large frequency range, voltage is higher than half of open volage. It is 1.2 kV under EC5 and 5.2 kV under EC8. Current also has a value of 16 A and 70 A under EC5 and EC8 respectively.

From the view of waveform amplitude, critical condition of voltage disturbance is more likely to appear in common mode due to large impedance. For current, it is more likely to appear in differential mode due to small impedance. Critical values are very close to immunity test levels. So, both voltage and current should be checked in case any one of them is out of limitation.

The following discusses the frequency domain spectrum and energy distribution for voltage and current waveforms. First, the spectrum and cumulative energy percentage of applied voltage into 50Ω are depicted in Fig. 16. To better observe the amplitude, the unit of the spectrum is set to be V/MHz.

For the voltage spectrum of EC5, the curve peak appears around 10 MHz. 90% of energy is concentrated between 7.9 MHz and 19.2 MHz. EC8 contains a larger frequency range of components, especially more in the low-frequency part. 90% of energy locates between 0.4 MHz and 20.2 MHz.

Similarly, spectrum and cumulative energy are calculated for voltage and current responses of different ports. The results under EC5 are shown in Fig. 17. Word C and D in brackets of the legend means Common mode (C) and Differential mode (D) respectively. It can be seen the spectrum peaks are still at 10 MHz. Low-frequency components are small for all ports. However, some ports have quite a portion of energy between 10 MHz and 100 MHz.

Results of the spectrum and cumulative energy of voltage and current under EC8 are presented in Fig. 18. The frequency range of components is much larger. The difference between different ports is also much larger than that in Fig. 17, especially for the cumulative energy of current in Fig. 18(d).

After making statistics for frequencies when cumulative energy reaches 5% and 95%, the results are obtained shown as in Fig. 19. Here, C and D in the X axis also means Common mode and Differential mode. For EC5 C, the frequency distribution is very concentrated. 5% frequency of voltage is 8.4 MHz to 8.6 MHz and 95% frequency is 16.4 MHz to 17.1 MHz. 5% frequency of current is 8.6 MHz to 9.2 MHz and 95% frequency is 43 MHz to 61.6 MHz. For EC5 D, 5% frequency values do not change much. It is 7.4 MHz to 9.2 MHz. 95% frequency of power and ethernet DC port goes up to 43.7 MHz and 64.4 MHz in Fig. 19(a). In Fig. 19(b), the value of the analog port goes up to 90.5 MHz, but other ports go down to about 20 MHz.

For EC8 C, frequencies are still concentrated for voltage. 5% value is much lower, about 0.19 MHz. 95% value is 16.4 MHz to

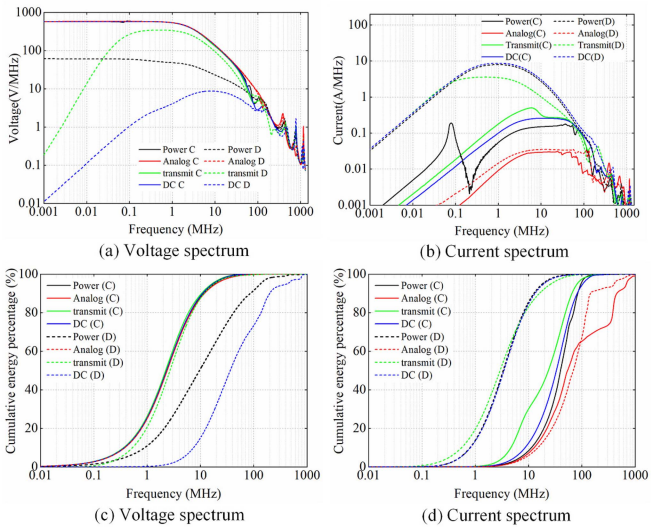

Fig. 18. Spectrum and cumulative energy of voltage and current under EC8.

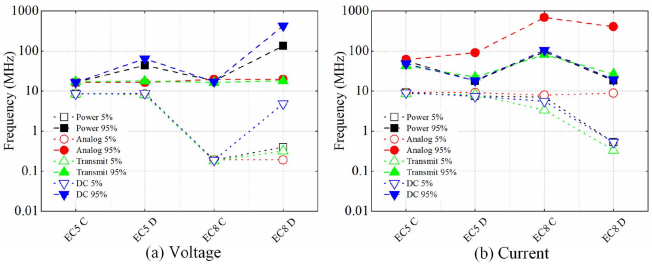

Fig. 19. 5% and 95% frequency under EC5 and EC8.

19.5 MHz. For the current, values are quite different. 5% value is 7.4 MHz to 9.2 MHz. 95% value of the analog port reaches 686 MHz. For EC8 D, values are more dispersed. 95% frequency of power and ethernet DC port is 134 MHz and 423 MHz for voltage. In Fig. 19(b), the analog port is different from others and 95% value goes up to 404 MHz.

C. Discussion About the Protection of PMU

The protection concept decides the selection of immunity test levels, which is related to line type, port type, and protection. Typically, disturbance on AC power cables is higher than on telecom cables and I/O data cables [32]. PCI simulation shows port voltage and current is related to port impedance and may have a large frequency range of components. Approximately, critical values are close to immunity test levels.

Additionally, if PMU is within poor shielding, the protection level will increase to a level with a much higher voltage, more than 10 kV, for both the power port and the I/O port [33]. There is a high probability that PMU will be damaged. Apart from the PMUs, the impedance modeling analyses can also provide insight into some fields of power systems, such as oscillation evaluation and suppression [34], [35].

Besides, if PMU is installed indoors with rebar shielding and nominal protection at the AC main, the 50% protection test level will be 8 kV for the power port and 2 kV for the I/O port. There is a probability that PMU will be damaged.

Additionally, if PMU is within poor shielding, the protection level will increase to a level with a much higher voltage, more than 10 kV, for both the power port and the I/O port. There is a high probability that PMU will be damaged.

If we intend to do a more targeted protection for some ports, then simulated voltage, current and energy distribution should be useful. They show the energy intensity and frequency range of conducted disturbance. This can provide support for selection of protection strategy and design of protection circuit.

VI. Conclusion

To explore the immunity of PMU devices in power systems under EMP, this article proposes an impedance measurement and the PCI testing scheme based on three instruments. Then, the nonuniform transmission line model is established to eliminate the effect of the fixture. After the de-embedding, all the measured impedance are integrated, and the results demonstrate the characteristics of different ports in PMU. Two pulse current generators are designed to generate damping sinusoid and double exponential waveform. By using port impedance as load, pulsed current injection simulation is further conducted to estimate the voltage and current response of PMU. The experimental results of the time domain waveforms, frequency domain spectrums, and cumulative energy distributions of the PCI testing reveal that different ports of PMU devices have different immune levels to EMP. Results can provide support for the corresponding protection strategy, such as an EMP shield.

Future work will focus on experimental verification to explore the degree of damage to different ports of PMU and failure probability.

References

[1] D. Slomovitz, L. Trigo, A. García, D. Izquierdo, C. Faverio, and R. Sandler, "A portable system for phasor measurment units (PMU) calibration in high-voltage substations," *Meas.: Sensors*, vol. 18, 2021, Art. no. 100329.

[2] W. Wang, K. Sun, C. Zeng, C. Chen, and Y. Liu, "Information and communication infrastructures in modern wide-area systems," in *Wide Area Power Systems Stability Protection and Security*, Berlin, Germany: Springer, 2020, pp. 71–104.

[3] S. S. Rangarajan, J. Sharma, D. P. Kothari, and T. Senjyu, "Novel utilization of phasor measurement units (PMU) in smart grid restoration: A brief survey," in *Advances in Smart Grid Automation and Industry 4.0*. Berlin, Germany: Springer, 2021.

[4] M. Panteli, D. N. Trakas, P. Mancarella, and N. D. Hatziargyriou, "Boosting the power grid resilience to extreme weather events using defensive islanding," *IEEE Trans. Smart Grid*, vol. 7, no. 6, pp. 2913–2922, Nov. 2016.

[5] B. J. Pierre, R. Guttromson, J. P. Eddy, R. Schiek, J. E. Quiroz, and M. J. Hoffman, "A framework to evaluate grid consequences from high altitude EMP events," 2020. [Online]. Available: https://www.osti.gov/biblio/1810043

[6] D. Wang, Y. Li, P. Dehghanian, and S. Wang, "Power grid resilience to electromagnetic pulse (EMP) disturbances: A literature review," in *Proc. North Amer. Power Symp.*, 2019, pp. 1–6.

[7] D. E. Sanabria, T. Bowman, R. Guttromson, M. Halligan, K. Le, and J. Lehr, "Early-time (E1) high-altitude electromagnetic pulse effects on trip coils," 2020. [Online]. Available: https://www.osti.gov/biblio/1714422

[8] X. Kong, Y.-Z. Xie, Q. Li, and Y.-H. Hu, "A multigap loop antenna and norm detector-based nano-second-level transient magnetic-field sensor," *IEEE Trans. Instrum. Meas.*, vol. 69, no. 10, pp. 8393–8400, Oct. 2020.

[9] R. Horton et al., "High-altitude electromagnetic pulse and the bulk power system, potential impacts and mitigation strategies," Electric Power Research Institute (EPRI), Palo Alto, CA, USA, Rep. no. 3002014979, 2019.
[10] MIL, "Requirements for the control of electromagnetic interference characteristics of subsystems and equipment (MIL-STD-461)," 2015. [Online]. Available: https://standards.nasa.gov/standard/NASA/MIL-STD-461
[11] H. M. Pennington, C. J. Hanley, and J. D. Rogers, "Toward an electromagnetic event resilient grid," *Proc. IEEE*, vol. 109, no. 4, pp. 315–319, Apr. 2021.
[12] Z. Cui, F. Grassi, and S. A. Pignari, "Circuit modeling of the test setup for pulsed current injection," in *Proc. AsiaPacific Int. Symp. Electromagn. Compat.*, 2016, pp. 726–728.
[13] Z. Cui, F. Grassi, S. A. Pignari, and B. Wei, "Pulsed current injection setup and procedure to reproduce intense transient electromagnetic disturbances," *IEEE Trans. Electromagn. Compat.*, vol. 60, no. 6, pp. 2065–2068, Dec. 2018.
[14] F. Grassi, F. Marliani, and S. A. Pignari, "Circuit modeling of injection probes for bulk current injection," *IEEE Trans. Electromagn. Compat.*, vol. 49, no. 3, pp. 563–576, Aug. 2007.
[15] X. Lu, G. Wei, X. Pan, X. Zhou, and L. Fan, "A pulsed differential-mode current injection method for electromagnetic pulse field susceptibility assessment of antenna systems," *IEEE Trans. Electromagn. Compat.*, vol. 57, no. 6, pp. 1435–1446, Dec. 2015.
[16] Z. Cui, B. Wei, F. Grassi, and S. A. Pignari, "Experimental analysis and circuit modeling of pulsed current injection in wire pairs," in *Proc. IEEE Int. Symp. Electromagn. Compat., IEEE AsiaPacific Symp. Electromagn. Compat.*, 2018, pp. 1109–1113.
[17] S. M. Ghania and A. M. Hashmi, "Transient overvoltages simulation due to the integration process of large wind and photovoltaic farms with utility grids," *IEEE Access*, vol. 9, pp. 43262–43270, 2021.
[18] K. Yamamoto, J. Takami, and N. Okabe, "Overvoltages on DC side of power conditioning system caused by lightning stroke to structure anchoring photovoltaic panels," *Elect. Eng. Jpn.*, vol. 187, no. 4, pp. 29–41, 2014.
[19] W. Qiu et al., "Port impedance measurement and current injection response analysis for PLCs," *IEEE Trans. Ind. Appl.*, vol. 58, no. 6, pp. 7838–7846, Nov./Dec. 2022.
[20] L. Callegaro, G. Konstantinou, C. A. Rojas, N. F. Avila, and J. E. Fletcher, "Testing evidence and analysis of rooftop PV inverters response to grid disturbances," *IEEE J. Photovolt.*, vol. 10, no. 6, pp. 1882–1891, Nov. 2020.
[21] P. G. Clem, E. Y. Wang, and J. D. Kotulski, "Emp-resilient electric grid transformer analysis," [Online]. Available: https://www.osti.gov/biblio/1684647
[22] L. Zhang et al., "Immunity study: Port impedance measurement of PMU and PCI testing under EMP," in *Proc. IEEE/IAS Ind. Commercial Power Syst. Asia*, 2022, pp. 800–805.
[23] R. Malaric, P. Mostarac, G. Petrovic, and J. Havelka, "Method for nonlinear fitting and impedance analysis with LCR meter," in *Proc. 23rd Int. Conf. Mixed Des. Integr. Circuits Syst.*," 2016, pp. 410–414.
[24] E. A. Szabo and Z. Park, "A unique extraction of metamaterial parameters based on Kramers-Kronig relationship," *IEEE Trans. Microw. Theory Techn.*, vol. 58, no. 10, pp. 2646–2653, Oct. 2010.
[25] A. M. Mangan, S. P. Voinigescu, M. T. Yang, and M. Tazlauanu, "De-embedding transmission line measurements for accurate modeling of IC designs," *IEEE Trans. Electron Devices*, vol. 53, no. 2, pp. 235–241, Feb. 2006.
[26] H. Ito and K. Masuy, "A simple through-only de-embedding method for on-wafer S-parameter measurements up to 110 GHz," in *Proc. IEEE MTT-S Int. Microw. Symp. Dig.*, 2008, pp. 383–386.
[27] M. F. Sultan, "Modeling of a bulk current injection setup for susceptibility threshold measurements," in *Proc. IEEE Int. Symp. Electromagn. Compat.*, 1986, pp. 1–8.
[28] IEC, "Electromagnetic compatibility (EMC) - Part 4-25: Testing and measurement techniques - HEMP immunity test methods for equipment and systems (IEC 61000-4-25)," 2019. [Online]. Available: https://webstore.iec.ch/publication/66249
[29] IEC, "Electromagnetic compatibility (EMC) - Part 2-10: Environment - description of HEMP environment - conducted disturbance (IEC 61000-2-10)," 2021. [Online]. Available: https://webstore.iec.ch/publication/61768
[30] IEC, "Electromagnetic compatibility (EMC) - Part 4-4: Testing and measurement techniques - Electrical fast transient/burst immunity test (IEC 61000-4-4)," 2012. [Online]. Available: https://webstore.iec.ch/publication/4222
[31] IEC, "Electromagnetic compatibility (EMC) - Part 4-18: Testing and measurement techniques - damped oscillatory wave immunity test (IEC 61000-4-18)," 2019. [Online]. Available: https://webstore.iec.ch/publication/60676
[32] IEC, "Electromagnetic compatibility (EMC) - Part 2-11: Environment - classification of HEMP environments (IEC 61000-2-11)," 1999. [Online]. Available: https://webstore.iec.ch/publication/4129
[33] National Coordinating Center for Communications (NCC), "Electromagnetic pulse (EMP) protection and resilience guidelines for critical infrastructure and equipment," 2019. [Online]. Available: https://www.cisa.gov/sites/default/files/publications/19_0307_CISA_EMP-Protection-Resilience-Guidelines.pdf
[34] K. Sun, W. Yao, J. Fang, X. Ai, J. Wen, and S. Cheng, "Impedance modeling and stability analysis of grid-connected DFIG-based wind farm with a VSC-HVDC," *IEEE Trans. Emerg. Sel. Topics Power Electron.*, vol. 8, no. 2, pp. 1375–1390, Jun. 2020.
[35] S. Zhao, R. Li, B. Gao, N. Wang, and X. Zhang, "Subsynchronous oscillation of PV plants integrated to weak AC networks," *IET Renewable Power Gener.*, vol. 13, no. 3, pp. 409–417, 2019.